Journal of Alloys and Compounds 765 (2018) 595–600

Contents lists available at ScienceDirect

Journal of Alloys and Compounds

journal homepage: http://www.elsevier.com/locate/jalcom

Suppression of crystallization in a Ca-based bulk metallic glass by compression

M. Naeem [a], S. Lan [a, b], B. Wang [a], X.Y. Wei [a], J. Zhou [c], Y. Ren [d], Z.P. Lu [c], D. Ma [e], A.D. Stoica [e], X.-L. Wang [a, f, *]

[a] Department of Physics, City University of Hong Kong, 83 Tat Chee Avenue, Kowloon, Hong Kong
[b] Herbert Gleiter Institute of Nanoscience, Nanjing University of Science and Technology, Nanjing, Jiangsu, 210094, China
[c] State Key Laboratory for Advanced Metals and Materials, University of Science and Technology Beijing, Beijing, 100083, China
[d] Advanced Photon Source, Argonne National Laboratory, Argonne, IL, 60439, USA
[e] Neutron Scattering Division, Spallation Neutron Source, Oak Ridge National Laboratory, Oak Ridge, TN, 37831, USA
[f] Center for Neutron Scattering, City University of Hong Kong Shenzhen Research Institute, Shenzhen Hi-Tech Industrial Park, Shenzhen, 518057, China

ARTICLE INFO

Article history:
Received 19 March 2018
Received in revised form
30 May 2018
Accepted 18 June 2018
Available online 19 June 2018

Keywords:
Bulk metallic glass
Crystallization
Annealing
Compression test
In-situ x-ray diffraction

ABSTRACT

We have studied the crystallization kinetics of $Ca_{40}Mg_{25}Cu_{35}$ bulk metallic glass under isothermal annealing in the supercooled liquid region, with and without applied stress, by *in-situ* high-energy synchrotron x-ray diffraction. We observed that without stress, crystallization started from the very beginning of isothermal annealing. However, when a uniaxial compressive stress was applied during isothermal annealing, no change in atomic order was observed at the beginning. Thereafter, the glassy structure relaxed, but still without noticeable evidence of crystallization. It is suggested that the applied compressive stress restricted the atomic mobility, which suppressed crystallization.

1. Introduction

Ca-based bulk metallic glasses (BMGs) are simple-metal based amorphous alloys with a very low density [1]. This feature, combined with low characteristic temperatures, low elastic modulus, and good glass-forming ability, makes Ca-based BMGs an excellent candidate for biomedical applications [1–7]. However, for biomedical applications, the stability of the amorphous structure is a major concern. Both temperature and stress can influence the glassy structure and cause crystallization [8]. It is crucial, therefore, to have a thorough understanding regarding modification of the structure with service time, under complex thermal and mechanical conditions. The superior mechanical and corrosion-resistant properties of BMGs are associated with the amorphous structures; crystallization can change the structure and hence deteriorate the intended functions. Although Ca-based BMGs were first reported in 2002 [2,3], and their atomic structure studies in the as-cast state have been reported with the help of x-ray and neutron diffraction as well as by *ab-initio* molecular dynamics and Reverse Monte Carlo simulations [9–11]. However, very few experimental studies (mostly post-mortem) have been conducted so far regarding their crystallization kinetics [12–14]. Moreover, there have been no prior *in-situ* studies of crystallization in BMGs under the combined effect of stress and temperature. Here, we report an *in-situ* isothermal annealing study in the supercooled liquid region (SCLR), with and without stress, for $Ca_{40}Mg_{25}Cu_{35}$ BMG by high-energy synchrotron x-ray scattering. After prolonged isothermal annealing, only partial crystallization took place; while under compressive stress, the extent of crystallization was negligible. The effect of compressive stress is explained in terms of reduced atomic mobility.

2. Experimental

Rod-shaped specimens of 3 mm in diameter and 6 mm in length were obtained from metallic glass ingots prepared by sintering, arc-melting, and suction-casting. Synchrotron high-energy x-ray

* Corresponding author. Department of Physics, City University of Hong Kong, 83 Tat Chee Avenue, Kowloon, Hong Kong.
E-mail address: xlwang@cityu.edu.hk (X.-L. Wang).

https://doi.org/10.1016/j.jallcom.2018.06.200
0925-8388/

diffraction (HE-XRD) was carried out at beamline 11-ID-C (E = 105 keV, λ = 0.11798 Å) of the Advanced Photon Source, Argonne National Laboratory, USA. $Ca_{40}Mg_{25}Cu_{35}$ BMG was selected for this study owing to its better glass-forming ability among the Ca-Mg-Cu alloy family. Differential scanning calorimetry (DSC) of the as-cast sample was conducted at a heating rate of 20 °C/min using Perkin-Elmer DSC7. From the DSC curve, a glass transition temperature T_g of 126 °C and onset of crystallization temperature T_x of 162 °C were obtained, thus providing a SCLR ($\Delta T_x = T_x - T_g$) of 36 °C. Synchrotron experiments were conducted *in-situ* under isothermal annealing in the SCLR at 135 °C (9 °C above T_g): (1) without load; (2) under uniaxial compression with a strain rate of 1.7×10^{-5} s^{-1} (maximum applied stress was approx. 180 MPa). Synchrotron x-ray data were recorded with a time interval of 7 s for the case without loading and 2 s for the experiment under load, with a total acquisition time of 6500 and 12690 s, respectively. FIT2D [15] was used for calibration with a standard CeO_2 sample and for conversion of 2D data to 1D. PDFgetX2 [16] was used for correction of data and for generation of the structure factor S(Q) and reduced pair distribution function G(r), where Q is the momentum transfer given by

$$Q = \frac{4\pi Sin\Theta}{\lambda}$$

G(r) is related to S(Q) by

$$G(r) = \frac{2}{\pi}\int_{Q_{min}}^{Q_{max}} Q[S(Q) - 1]Sin(Qr)dQ$$

Corrections were applied for sample background, sample self-absorption, Compton scattering, x-ray polarization, energy dependence, etc. The exact wavelength (0.11798 Å), sample composition ($Ca_{40}Mg_{25}Cu_{35}$, in atomic percent), sample thickness (3 mm), number density (0.03987 Atoms/$Å^3$), and sample geometry (flat plate transmission) was used. For the kinetic study data, to construct the integration intensity plots [Figs. 2(c) and 3(e)] from a large number of data points, PDFgetX3 [17] was used after benchmarking selective sets of data with PDFgetX2.

3. Results and discussion

The evolution of the S(Q) for $Ca_{40}Mg_{25}Cu_{35}$ BMG during isothermal annealing at 135 °C and under compression at 135 °C (hereafter referred to as annealing and loading conditions, respectively, in the rest of the text for simplicity) are presented in Fig. 1. Although the S(Q) data were collected up to a Q_{max} of 35 $Å^{-1}$, only data up to a maximum Q of 12 $Å^{-1}$ are shown for clarity. The initial (as-cast) patterns for both samples showed a pre-peak, which is attributed to the presence of extended medium-range order in the amorphous alloys [18–21]. The pre-peak remained prominent till the end of the experiment under both annealing and loading conditions.

The first sharp diffraction peak (FSDP) is asymmetrical in shape and is located in the Q-range of 1.80–3.37 $Å^{-1}$ with the peak center at 2.35 $Å^{-1}$. Significant changes can be seen in S(Q) after 2000 s of isothermal annealing in comparison to the initial pattern [Fig. 1(a)]. The FSDP broadened with annealing time and ultimately split into two peaks, which indicates the formation of a crystalline phase [22]. After FSDP, the appearance of a kink at 3.2 $Å^{-1}$ also signifies the development of structural order in the system. The appearance of crystalline peaks can also be seen in the Q range of 4.0–8.0 $Å^{-1}$. Crystallization started developing rapidly from the very beginning of the experiment, but the rate of crystallization slowed down with

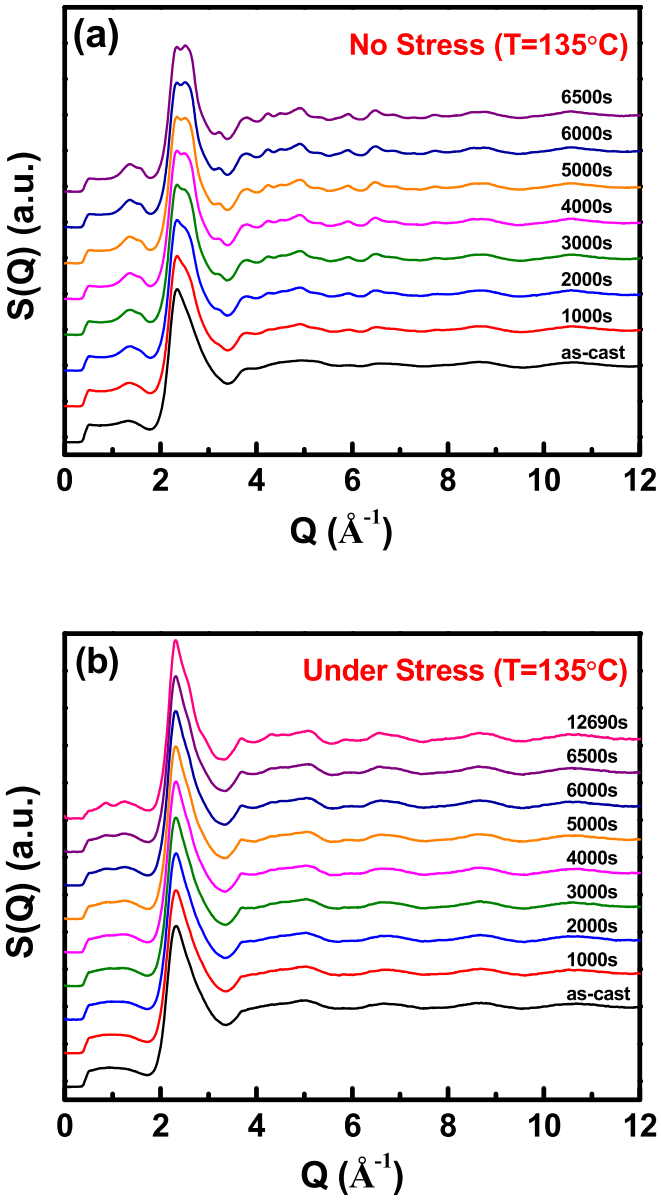

Fig. 1. Structure factor evolution of $Ca_{40}Mg_{25}Cu_{35}$ BMG during isothermal annealing at 135 °C (**a**), and under compression while isothermally annealing at 135 °C (**b**).

increasing annealing time and only minor changes happened after 3000 s. Towards the end of the experiment, the crystalline peaks are few in number and still very broad, which indicates that sample is only partially crystallized.

Another sample of the same composition was subjected to compressive stress in addition to isothermal annealing at 135 °C. Surprisingly, it showed very little change [see Fig. 1(b)] in comparison to the case of isothermal annealing alone. The FSDP did not show any broadening or splitting, and no new peak appeared during the long loading time of 12690 s. It is thus concluded that the applied compressive stress suppressed the crystallization.

Fig. 2 compares the evolution of FSDP for both experiments. Under annealing alone, as illustrated in Fig. 2(a), a significant shoulder peak developed as a result of crystallization. Fig. 2(b) shows the behavior of FSDP under load; it remained essentially unchanged except an increase in the peak intensity which is associated with relaxation of the glassy structure [22]. Under

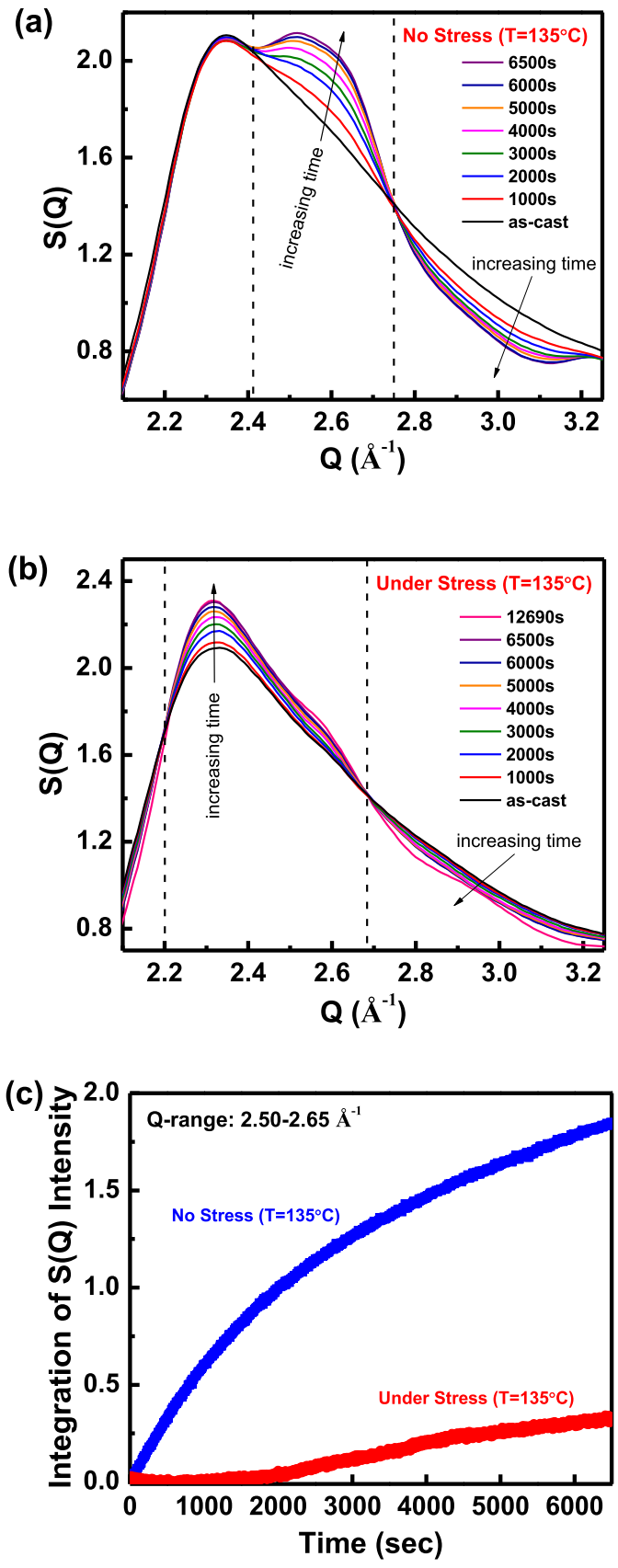

Fig. 2. Changes in FSDP during the course of the annealing experiments: (**a**) without load showing two sub-peaks due to crystallization, (**b**) under loading where the structure relaxation was observed as evidenced by sharpening of the FSDP, (**c**) variation of integrated S(Q) peak intensity during annealing and straining.

annealing alone, the FSDP started to broaden from the top, which ultimately transformed to a shoulder peak, and gave rise to three distinct Q-regions as marked by vertical dashed lines in Fig. 2(a). In the low-Q region ($Q < 2.41$ Å^{-1}), the S(Q) remained essentially unaffected by annealing. The intensity in the middle-Q region ($Q = 2.41–2.75$ Å^{-1}) kept increasing and this leads to a new shoulder peak after splitting at 2.41 Å^{-1}. The growth of this phase can be seen with annealing time. The intensity increase in this region occurred due to nucleation, but because of small crystallite size the shoulder peak remained broad in the beginning and finally split into two peaks, which is a clear indication of a new phase. Between 2.75 and 3.20 Å^{-1}, the intensity decreased with annealing time and the growth of the new phase happened at the expense of this Q region. Fig. 2(b) shows the behavior of FSDP under loading. It also consists of three distinct regions: (i) peak narrowing until 2.20 Å^{-1}; (ii) increase in intensity between 2.20 and 2.68 Å^{-1}; and (iii) narrowing of peak for $Q > 2.68$ Å^{-1}. However, here, the increase in intensity and narrowing of the peak is due to the relaxation of the glassy structure [22]. In the loading scenario, the absence of any shoulder peak indicates the lack of significant crystallization.

Fig. 2(c) is a comparison of FSDP integrated intensity for both experiments, over the Q-range of 2.50–2.65 Å^{-1}. Under isothermal annealing, crystallization started from the very beginning, upon reaching the annealing temperature, with a fast growth rate for the first 1200 s. On the other hand, when a stress was applied during isothermal annealing, no change in intensity was observed for the first 1500 s and even when S(Q) intensity started to increase at the later time, the rate of change was extremely slow.

The PDF G(r) graphs are presented in Fig. 3(a) and (b). The first PDF peak, which characterizes the nearest-neighbors or the short-range order (SRO) [23], exhibits three shoulders at 2.54 Å, 3.06 Å and 3.72 Å, which corresponds to Cu-Cu, Cu-Ca and Ca-Ca atomic pairs, respectively [9–11], as highlighted in Fig. 3(c) and (d). The contribution from Mg-Mg pair can be ignored due to the relatively low concentration of Mg and its small atomic number while Cu-Mg and Mg-Ca pairs are overlapped with others [9]. The Cu-Ca peak shifts to a larger r value during isothermal annealing but no such change was observed when a compressive stress was applied, see Fig. 3(c) and (d).

In Fig. 3(a), the second G(r) peak ($r = 4.4–7.1$ Å) became sharp with increasing annealing time. An additional peak centered at 6.75 Å appeared at the tail of the second peak and its intensity increased steadily with the annealing time. The second PDF peak and beyond characterizes the medium-range order (MRO) and thus the observed changes signifies the development of the MRO [24]. Additional new peaks developed at larger r values indicate the formation of new bonds. Note that the sample was only partially crystallized after 6500 s of annealing, as the peaks were still fairly broad.

Fig. 3(b) shows the effect of stress on G(r) patterns. Changes above the MRO scale are quite different from the annealing scenario. For example, no additional peak developed at 6.75 Å under stress. Additionally, no shifting of the central peak of SRO was observed either, see Fig. 3(d). Under stress, the changes from the initial pattern were negligible, despite the fact that the sample was subjected to stress (with annealing) for much longer duration than isothermal annealing alone.

Fig. 3(e) presents the variation of integrated intensities for $r = 11.88–12.13$ Å (the position marked with arrows in Fig. 3(a) and (b)). The intensity was almost unchanged with time under the compressive stress while a steady build-up of intensity in the absence of load can be seen. The development of medium-to-long range order is evident in the absence of load, whereas little change was observed under a compressive stress. It can be inferred that the uniaxial compressive stress when applied in the SCLR,

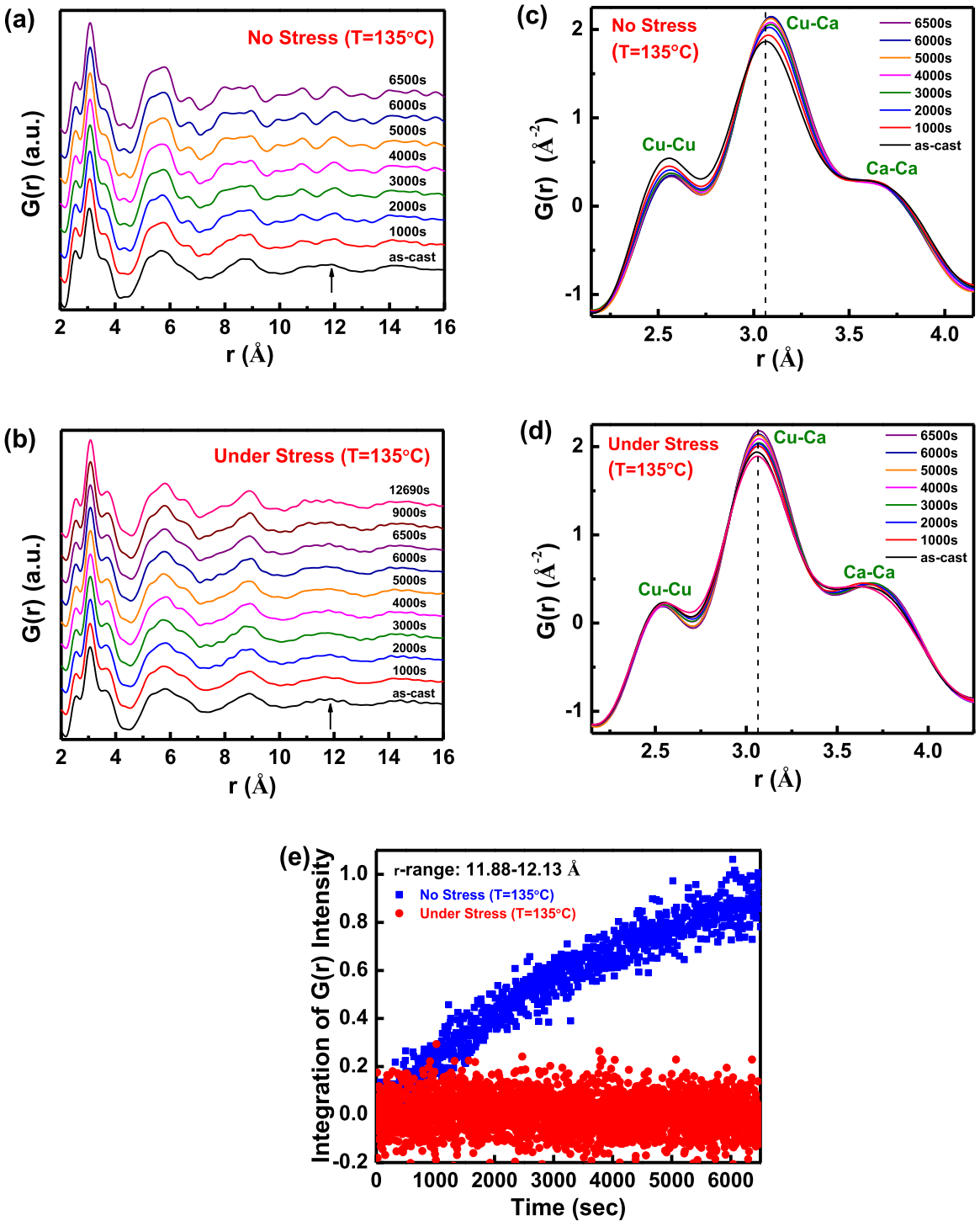

Fig. 3. PDF under annealing (**a**), and under stress (**b**), in the SCLR. The first PDF peak consisting of three sub-peaks corresponding to different atomic pairs are presented for both scenarios (**c**)–(**d**). Comparison of integrated PDF peak intensity is shown in (**e**).

inhibited the development of long-range order in the system by restricting the atomic mobility (evident from little shift of the central shoulder peak in Fig. 3(d)).

The suppression of crystallization under compression is unusual as stress can facilitate crystallization in MGs, especially since temperature and stress have been demonstrated [25,26] to give rise to equivalent effects on the structure. On the other hand, it has been reported that hydrostatic pressure tends to stabilize the glassy structure. Xue et al. [27] recently demonstrated the enhancement in the stability of BMG by applying pressure at room temperature, which led to an upward shift in T_g and T_x. Moreover, their sample remained stable even when heated well above T_g temperature. Jiang et al. [28] also observed an increase in T_x under high pressure and attributed the retardation of crystallization to restriction in

atomic mobility under high pressure, leading to larger thermal activation energy required for crystallization to take place. However, in the case of uniaxial compression both pressure and shear stress play a role. Whereas the pressure increases viscosity and retarding the flow, the shear stress tends to enhance the flow by breaking the atomic bonds [26,27,29,30]. The present experiment was conducted at a temperature above T_g, where the effect of shear is diminishing. Therefore, in our study of Ca-based BMG, the pressure is expected to play a dominant role.

The nucleation rate, *I*, for continuous nucleation is given by [31]:

$$I \propto \mathrm{D.e}\left(-\frac{W^*}{k_B T}\right) \quad (1)$$

where D is diffusion coefficient, W* is nucleation barrier, k_B is Boltzmann constant, and T is the absolute temperature. Nucleation barrier, W*, can be expressed in terms of interfacial energy (σ) and the chemical potential (Δg): $W^* = \frac{16\pi}{3}\frac{\sigma^3}{(\Delta g)^2}$. From Equation (1), the nucleation rate is proportional to the diffusion coefficient. Under the influence of compressive stress, the diffusion and hence the atomic mobility will be restricted. As a result, the nucleation rate will be slower, compared to the case where no stress is applied. Meanwhile, it should be noted that a compressive stress in the vicinity of T_g could produce an inhomogeneous strain field, leading to an increased interfacial energy, σ. As Equation (1) shows, a large σ also suppresses nucleation and hence the crystallization.

It should be noted that the effect of pressure also depends on the alloying elements. Guo and Li conducted a simulation study of phase transitions in amorphous solids under hydrostatic compression [32]. It was found that under pressure, the free volume is reduced because of compression of soft atoms. This lead to a slow-down diffusion or atomic mobility, which stabilized the glass structure. However, the effect of compressive stress is atomic size dependent. Large atoms are soft centers and therefore are more compressible, whereas small atoms are hard centers and incompressible [32]. In Ca-Mg-Cu BMG, Ca atoms are large atoms and considered soft, whereas Cu atoms are small and hence hard. The PDF analysis provided supporting evidence in that under isothermal annealing, the central PDF peak position moved from 3.06 Å to 3.09 Å, while under a compressive load there was essentially no change in the peak position [Fig. 3(c) and (d)], demonstrating the effect of pressure on restraining the atomic mobility.

4. Conclusions

In summary, crystallization kinetics of the ternary $Ca_{40}Mg_{25}Cu_{35}$ BMG were studied by *in-situ* synchrotron x-ray diffraction under two conditions above the glass transition temperature: (1) isothermal annealing and (2) uniaxial compression with isothermal annealing. In the case of isothermal annealing, crystallization was fast at the beginning of the experiment, but after initial crystallization, the rate slowed down, and the sample was only partially crystalline after 6500 s of annealing. However, under a compressive stress in conjunction with isothermal annealing, relaxation of the glass structure was observed without noticeable crystallization, even after 12690 s of loading in the SCLR. Apparently, the pressure component dominated in the competing shearing vs. pressure effect, thus restricting atomic diffusion beyond nearest-neighbors and inhibiting the development of medium-to-long range order, which took place in the absence of stress. It would be valuable to investigate crystallization pathways of other Ca-based BMG alloys as well as to carry out atomistic studies by computer simulations on the underlying mechanism which caused suppression of crystallization under compressive stress.

Acknowledgements

Insightful discussions with Profs. Takeshi Egami and Mo Li are gratefully acknowledged. The work was supported by a grant from the Research Grants Council of the Hong Kong Special Administrative Region [CityU Project No. 11216215] and National Natural Science Foundation of China [Project No. 51571170, 51501090]. X.L.W. acknowledges the support by the National Key R&D Program by the Ministry of Science and Technology (MOST) of China (Grant No. 2016YFA0401501). The synchrotron X-ray work used resources of the Advanced Photon Source, a US Department of Energy (DOE) Office of Science User Facility operated by Argonne National Laboratory under Contract No. DE-AC02-06CH11357.

References

[1] J.-Z. Jiang, D. Hofmann, D.J. Jarvis, H.-J. Fecht, Low-density high-strength bulk metallic glasses and their composites: a review, Adv. Eng. Mater. 17 (2015) 761–780, https://doi.org/10.1002/adem.201400252.
[2] K. Amiya, A. Inoue, Formation, thermal stability and mechanical properties of Ca-based bulk glassy alloys, Mater. Trans. 43 (2002) 81–84, https://doi.org/10.2320/matertrans.43.81.
[3] K. Amiya, A. Inoue, Formation and thermal stability of Ca-Mg-Ag-Cu bulk glassy alloys, Mater. Trans. 43 (2002) 2578–2581, https://doi.org/10.2320/matertrans.43.2578.
[4] O.N. Senkov, D.B. Miracle, V. Keppens, P.K. Liaw, Development and characterization of low-density Ca-Based bulk metallic glasses: an overview, Metall. Mater. Trans. A 39 (2008) 1888–1900, https://doi.org/10.1007/s11661-007-9334-z.
[5] O.N. Senkov, J.M. Scott, D.B. Miracle, Composition range and glass forming ability of ternary Ca–Mg–Cu bulk metallic glasses, J. Alloys Compd. 424 (2006) 394–399, https://doi.org/10.1016/j.jallcom.2006.01.104.
[6] V. Keppens, Z. Zhang, O.N. Senkov, D.B. Miracle, Localized Einstein modes in Ca-based bulk metallic glasses, Philos. Mag. 87 (2007) 503–508, https://doi.org/10.1080/14786430600857353.
[7] J.D. Cao, N.T. Kirkland, K.J. Laws, N. Birbilis, M. Ferry, Ca-Mg-Zn bulk metallic glasses as bioresorbable metals, Acta Biomater. 8 (2012) 2375–2383, https://doi.org/10.1016/j.actbio.2012.03.009.
[8] H.F. Li, Y.F. Zheng, Recent advances in bulk metallic glasses for biomedical applications, Acta Biomater. 36 (2016) 1–20, https://doi.org/10.1016/j.actbio.2016.03.047.
[9] E.R. Barney, A.C. Hannon, O.N. Senkov, J.M. Scott, D.B. Miracle, R.M. Moss, A neutron and X-ray diffraction study of Ca-Mg-Cu metallic glasses, Intermetallics 19 (2011) 860–870, https://doi.org/10.1016/j.intermet.2011.02.001.
[10] O.N. Senkov, Y.Q. Cheng, D.B. Miracle, E.R. Barney, A.C. Hannon, C.F. Woodward, Atomic structure of Ca40+XMg25Cu35−X metallic glasses, J. Appl. Phys. 111 (2012) 123515, https://doi.org/10.1063/1.4729450.
[11] O.N. Senkov, Y.Q. Cheng, Ab initio molecular dynamics simulation of the amorphous structure of Ca-Mg-Cu and Ca-Mg-Zn alloys, Metall. Mater. Trans. A 44 (2013) 1980–1989, https://doi.org/10.1007/s11661-012-1406-z.
[12] D. Okai, M. Inoue, T. Mori, T. Fukami, T. Yamasaki, H.M. Kimura, et al., Annealing effect on mechanical constants for Ca48Mg27Cu25bulk metallic glass, J. Alloys Compd. 504 (2010) S95–S97, https://doi.org/10.1016/j.jallcom.2010.03.103.
[13] D. Okai, Y. Shimizu, N. Hirano, T. Fukami, T. Yamasaki, A. Inoue, Isothermal crystallization in supercooled liquid state for Ca50Mg22.5Cu27.5metallic glass, J. Alloys Compd. 504 (2010) S247–S250, https://doi.org/10.1016/j.jallcom.2010.03.225.
[14] L. Hu, F. Ye, Crystallization kinetics of Ca65Mg15Zn20 bulk metallic glass, J. Alloys Compd. 557 (2013) 160–165, https://doi.org/10.1016/j.jallcom.2012.12.158.
[15] A.P. Hammersley, S.O. Svensson, M. Hanfland, A.N. Fitch, D. Hausermann, Two-dimensional detector software: from real detector to idealised image or two-theta scan, High Press. Res. 14 (1996) 235–248, https://doi.org/10.1080/08957959608201408.
[16] X. Qiu, J.W. Thompson, S.J.L. Billinge, PDFgetX2: a GUI-driven program to obtain the pair distribution function from X-ray powder diffraction data, J. Appl. Crystallogr. 37 (2004) 678, https://doi.org/10.1107/S0021889804011744.
[17] P. Juhás, T. Davis, C.L. Farrow, S.J.L. Billinge, PDFgetX3: a rapid and highly automatable program for processing powder diffraction data into total scattering pair distribution functions, J. Appl. Crystallogr. 46 (2013) 560–566, https://doi.org/10.1107/S0021889813005190.
[18] W. Hoyer, R. Jödicke, Short-range and medium-range order in liquid Au-Ge alloys, J. Non Cryst. Solids 192–193 (1995) 102–105. https://doi.org/10.1016/0022-3093(95)00335-5.
[19] L. Zhang, Y. Wu, X. Bian, H. Li, W. Wang, S. Wu, Short-range and medium-range order in liquid and amorphous Al90Fe5Ce5 alloys, J. Non Cryst. Solids 262 (2000) 169–176. https://doi.org/10.1016/S0022-3093(99)00699-7.

[20] N.A. Mauro, V. Wessels, J.C. Bendert, S. Klein, A.K. Gangopadhyay, M.J. Kramer, et al., Short- and medium-range order in Zr80Pt20 liquids, Phys. Rev. B 83 (2011) 184109, https://doi.org/10.1103/PhysRevB.83.184109.
[21] Y.Q. Cheng, E. Ma, Atomic-level structure and structure-property relationship in metallic glasses, Prog. Mater. Sci. 56 (2011) 379–473, https://doi.org/10.1016/j.pmatsci.2010.12.002.
[22] G. D'Angelo, C. Crupi, M.A. Gonzalez, E. Basile, V.C. Nibali, C. Mondelli, Prepeak and first sharp diffraction peak in the structure factor of (Cs2O)0.14(B2O3) 0.86 glass: influence of temperature, J. Phys. Chem. B 114 (2010) 12565–12571, https://doi.org/10.1021/jp1005555.
[23] T. Egami, S.J.L. Billinge, Underneath the Bragg Peaks: Structural Analysis of Complex Materials, Pergamon, 2003.
[24] S. Lan, Y. Ren, X.Y. Wei, B. Wang, E.P. Gilbert, T. Shibayama, et al., Hidden amorphous phase and reentrant supercooled liquid in Pd-Ni-P metallic glasses, Nat. Commun. 8 (2017) 14679, https://doi.org/10.1038/ncomms14679.
[25] H.L. Peng, M.Z. Li, W.H. Wang, Stress-versus temperature-induced structural evolution in metallic glasses, Appl. Phys. Lett. 102 (2013) 131908, https://doi.org/10.1063/1.4800531.
[26] P. Guan, M. Chen, T. Egami, Stress-temperature scaling for steady-state flow in metallic glasses, Phys. Rev. Lett. 104 (2010) 205701, https://doi.org/10.1103/PhysRevLett.104.205701.
[27] R.J. Xue, L.Z. Zhao, C.L. Shi, T. Ma, X.K. Xi, M. Gao, et al., Enhanced kinetic stability of a bulk metallic glass by high pressure, Appl. Phys. Lett. 109 (2016) 221904, https://doi.org/10.1063/1.4968834.
[28] J.Z. Jiang, T.J. Zhou, H. Rasmussen, U. Kuhn, J. Eckert, C. Lathe, Crystallization in Zr41.2Ti13.8Cu12.5Ni10Be22.5 bulk metallic glass under pressure, Appl. Phys. Lett. 77 (2000) 3553, https://doi.org/10.1063/1.1328375.
[29] T. Iwashita, T. Egami, Atomic mechanism of flow in simple liquids under shear, Phys. Rev. Lett. 108 (2012) 196001, https://doi.org/10.1103/PhysRevLett.108.196001.
[30] C. Chen, M. Gao, C. Wang, W.-H. Wang, T.-C. Wang, Fracture behaviors under pure shear loading in bulk metallic glasses, Sci. Rep. 6 (2016) 39522, https://doi.org/10.1038/srep39522.
[31] K.F. Kelton, A.L. Greer, Nucleation in Condensed Matter : Applications in Materials and Biology, Pergamon, 2010.
[32] Y.Z. Guo, M. Li, Equation of state and topological transitions in amorphous solids under hydrostatic compression, J. Appl. Phys. 108 (2010) 113510, https://doi.org/10.1063/1.3512913.